



**$x$ -[Pd(dmit)<sub>2</sub>]<sub>2</sub> as a quasi-one-dimensional scalene Heisenberg model**E. P. Kenny <sup>\*</sup>, A. C. Jacko, and B. J. Powell*School of Mathematics and Physics, The University of Queensland, Brisbane, Queensland 4072, Australia* (Received 6 April 2021; revised 7 July 2021; accepted 16 August 2021; published 30 August 2021)

From first principles, we calculate the Heisenberg interactions between neighboring dimers in several compounds within the  $\text{Et}_n\text{Me}_{4-n}\text{X}[\text{Pd}(\text{dmit})_2]_2$  (Et = ethyl, Me = methyl, dmit = 2-thioxo-1,3-dithiole-4,5-dithiolate) family using an atomistic approach, with broken-symmetry density functional theory. In all materials, we find a scalene triangular model where the strongest exchange coupling along one crystallographic axis is up to three times larger than the others and where the frustration further enhances this quasi-one-dimensionality. We calculate the Néel ordering temperature via the chain random phase approximation. We show that the difference in the frustrated interchain couplings is equivalent to a single bipartite interchain coupling, favoring long-range magnetic order. We find that the Néel ordering temperatures are the same order of magnitude as the experimentally measured values for most compounds.

DOI: [10.1103/PhysRevMaterials.5.084412](https://doi.org/10.1103/PhysRevMaterials.5.084412)**I. INTRODUCTION**

Charge transfer salts, especially the  $\text{Et}_n\text{Me}_{4-n}\text{X}[\text{Pd}(\text{dmit})_2]_2$  ( $x$ -[Pd(dmit)<sub>2</sub>]<sub>2</sub>) family, have been of intense interest for more than a decade. Geometric frustration and strong electron correlations lead to a wide range of exotic phenomena [1,2]. All  $x$ -[Pd(dmit)<sub>2</sub>]<sub>2</sub> compounds are Mott insulators at ambient pressure and low temperature, but changing the counter-ion ( $X$  and  $n$ ) leads to many different ground states. Most salts exhibit antiferromagnetic order, for example,  $X$ - $n$  = As-0, As-1, As-2, N-0, and Sb-0 [3–5]. Others exhibit valence-bond order (P-1) [6,7], charge order (Sb-2) [8,9], and spin-liquid behavior (Sb-1) [10–13]. Those with antiferromagnetic order have been shown to exhibit unconventional superconducting behavior with the application of hydrostatic pressure or uniaxial strain [14,15]. Regardless of their ground state, most compounds in this family exhibit magnetic ordering at a temperature much lower than is expected based on the strength of their magnetic interactions.

All compounds contain isomorphous layers of Pd(dmit)<sub>2</sub> dimers separated by layers of counter-ions. The Pd(dmit)<sub>2</sub> dimers are arranged in a geometrically frustrated, scalene triangular lattice, differing only slightly between compounds. A single Pd(dmit)<sub>2</sub> layer is shown in Fig. 1. The dimers form “stacks” along the (1,1,0) lattice direction (along the horizontal in the figure). All of the materials studied here, except for P-1, are the so-called solid crossing bilayer alternate where, in successive layers, the stacks are along the (1,1,0) and (1,1̄,0) directions. In P-1, all layers are equivalent and stack along the (1,1,0) lattice direction.

Their behavior above and below the Mott transition can be well described by a Hubbard model and, in the insulating phase, a Heisenberg model [1]. In the insulating phase, there is

one unpaired electron on each dimer. *Ab initio* calculations on these compounds, including the parametrization of effective models, are difficult because of their chemical complexity (with  $\sim 300$  atoms per unit cell). In effective spin models, each spin site is an entire Pd(dmit)<sub>2</sub> monomer or dimer.

Previous studies of  $x$ -[Pd(dmit)<sub>2</sub>]<sub>2</sub> have parameterized tight-binding models on the basis of band structure calculations by fitting or via Wannier functions centered on monomers or dimers [1,16–21]. Extracting tight-binding parameters from band structure calculations relies on Kohn-Sham eigenvalues. These do not correspond to nature, but are rather an internal density functional theory (DFT) device for calculating the total density [22]. Kohn-Sham eigenvalues often poorly reproduce energy differences, even in weakly correlated materials [23,24], and dramatically fail in strongly correlated materials [25]. For example, in Sb-1, the Kohn-Sham band structure is metallic [1,17–20] rather than insulating, as in experiment [1,2].

Due to the large unit cell, periodic calculations on these compounds reduce the choice of exchange-correlation functionals. Most previous periodic DFT studies of these compounds [17–21] are based on pure density functionals, i.e., the local density approximation (LDA) or generalized gradient approximation (GGA). These functionals are known to perform poorly for parametrizing magnetic interactions [26–29]—particularly superexchange [30].

In this paper, we present a first-principles study of the magnetic interactions within several  $x$ -[Pd(dmit)<sub>2</sub>]<sub>2</sub> compounds ( $X$ - $n$  = Sb-0, Sb-1, As-0, As-1, As-2, N-0, P-1) using broken-symmetry density functional theory (BS-DFT). Although there is a trade-off in accuracy when using a nonperiodic approach in a crystal [26,31–34], BS-DFT has advantages in contrast to the methods employed in previous studies. BS-DFT makes use of ground-state energy differences, which have a formal basis in DFT (the Hohenberg-Kohn theorem [35]) and are much more accurate in DFT than the Kohn-Sham eigenvalues. Moreover, it allows us to directly determine the

<sup>\*</sup>elisekenny@gmail.com

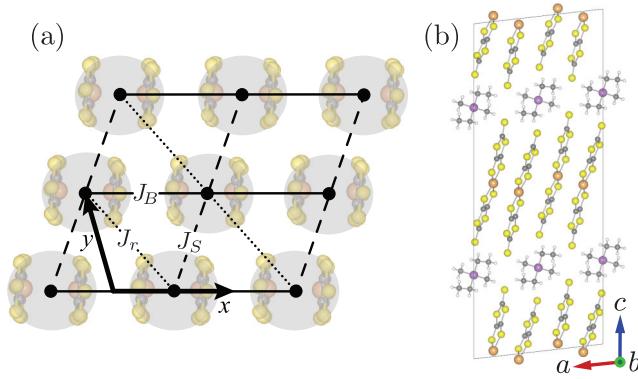


FIG. 1. (a) The intralayer geometry of  $x$ -[Pd(dmit)<sub>2</sub>]<sub>2</sub>. Each layer forms a scalene (anisotropic) triangular lattice of dimers with interdimer exchange couplings  $J_B$ ,  $J_r$ , and  $J_S$  as shown. We find that  $J_B$ , along the dimer stacking direction, is the largest for all compounds in this paper. (b) The unit cell of As-2, showing the layered structure perpendicular to the [Pd(dmit)<sub>2</sub>]<sub>2</sub> layers shown in (a).

Heisenberg exchange interaction, rather than extracting the magnetic behavior from tight-binding [18–20] or Hubbard [17,21] models, where the electron-electron interaction parameters are often poorly known.

We find an effective Heisenberg model that is quasi-one-dimensional (one interaction, along the stacking direction, is much larger than the others). We then compare our model to experimental results using the chain random phase approximation (CRPA) together with the exact form of the dynamical susceptibility for a one-dimensional chain to calculate the Néel ordering temperature for each compound.

In the past, these materials have been analyzed and modeled through a quasi-two-dimensional picture [1,2]. This paradigm stems from early calculations of dimer-dimer electron transfer integrals  $t_B$ ,  $t_S$ , and  $t_r$  (cf. Fig. 1) using an extended Hückel molecular orbital method, resulting in  $t_B \approx t_S > t_r$  [14]. This two-dimensional (2D) picture was reinforced by approximate fits of the 2D triangular Heisenberg model to the magnetic susceptibility data [16,36,37]. However, *ab initio* investigations using more sophisticated methods such as DFT have suggested that for most compounds,  $t_B > t_S \approx t_r$  [19,21]. Recently, BS-DFT has been used to parametrize a spin model for the spin-liquid candidate Sb-1, with the finding that  $J_B \gg J_S \approx J_r$  [38]. The BS-DFT calculations we present here confirm this result for many other compounds in the  $x$ -[Pd(dmit)<sub>2</sub>]<sub>2</sub> family. Hence, we argue that they should all be understood as quasi-one-dimensional.

Our calculations reveal that in all materials, the strongest exchange coupling is along the dimer stacking direction ( $J_B$ ; cf. Fig. 1). This leads to a quasi-one-dimensional Hamiltonian. Modeling these compounds via a quasi-1D approach allows us to calculate their Néel ordering temperatures analytically. Specifically, we use the chain random phase approximation (CRPA) around the large  $J_B$  limit, starting from the exact form for the one-dimensional magnetic susceptibility of a Heisenberg spin-1/2 chain and treating interchain interactions via the RPA [39,40]. In the case of an isosceles triangular lattice, the interchain interactions are perfectly frustrated. This suppresses ordering at any

temperature [40,41] within the CRPA. In  $x$ -[Pd(dmit)<sub>2</sub>]<sub>2</sub>, we find that the anisotropy in the interchain coupling leads to an effective unfrustrated interchain interaction, given by the difference of the interchain couplings ( $\delta J_y = J_r - J_S$ ).

The Heisenberg exchange interaction  $J_{ij}$  mainly arises from two different physical contributions—superexchange (SE) and direct exchange (DE),  $J_{ij} = J_{ij}^{SE} + J_{ij}^{DE}$ . In molecular crystals such as  $x$ -[Pd(dmit)<sub>2</sub>]<sub>2</sub>,  $J_{ij}^{SE}$  is often the largest term [17,21,38]. It arises from virtual hopping processes and usually favors antiferromagnetism [42]. This interaction is encompassed by the Hubbard model.  $J_{ij}^{DE}$  arises from the antisymmetry of electron wave functions. It favors ferromagnetism and depends mostly on the distance between sites. Superexchange and direct exchange are usually of opposite sign; a significant direct exchange can counteract the superexchange interaction and lower the magnitude of  $J_{ij}$ . Estimates of  $J_{ij}$  from Hückel and DFT band structure calculations typically neglect  $J_{ij}^{DE}$ . However, studies that have calculated  $J_{ij}^{DE}$  directly have found that its magnitude is significant in these compounds [3,21,38]. For this reason, studies that take direct exchange into account are bound to be more successful at accurately modeling experimental behaviors in  $x$ -[Pd(dmit)<sub>2</sub>]<sub>2</sub>. Since we directly calculate the total  $J_{ij}$  in this work, all its contributions (including superexchange and direct exchange) are present in our modeling.

## II. PARAMETRIZATION OF HEISENBERG MODEL WITH BS-DFT

We directly parametrize a Heisenberg model,

$$\mathcal{H} = \sum_{ij} J_{ij} \mathbf{S}_i \cdot \mathbf{S}_j, \quad (1)$$

where  $\mathbf{S}_i$  is the spin operator on the  $i$ th dimer and  $J_{ij}$  are the exchange coupling constants.

The exchange couplings  $J_{ij}$  are calculated as the energy difference between specific spin states of each tetramer in the compound—using BS-DFT along with the Yamaguchi spin decontamination procedure. In this approach [43–45],

$$J_{ij} = 2 \frac{E_{ij}^T - E_{ij}^{BS}}{\langle S^2 \rangle_{ij}^T - \langle S^2 \rangle_{ij}^{BS}}, \quad (2)$$

where  $E_{ij}^T$  is the triplet energy of the isolated tetramer (two neighboring dimers,  $i$  and  $j$ ) and  $E_{ij}^{BS}$  is the energy of the broken-symmetry state, where the unpaired spins on each dimer are misaligned.  $\langle S^2 \rangle_{ij}^{BS}$  and  $\langle S^2 \rangle_{ij}^T$  are the corresponding expectation values of the spin operator,  $S^2$ . In cases of large spin contamination, the Yamaguchi approach has been shown to lead to inaccurate results [46], in which case other mapping procedures are preferable [26,31–34]. However, we find that  $\langle S^2 \rangle_{ij}^T - \langle S^2 \rangle_{ij}^{BS}$  has a maximum value of 1.16, indicating a small amount of spin contamination (see Supplemental Material [47]). The coordinates for each tetramer included two Pd(dmit)<sub>2</sub> dimers and the six closest counter-ions. Calculations were performed in GAUSSIAN09 [48] with the uB3LYP functional [49,50] and using the LANL2DZ [51–54] (for Pd, Sb, As, and Cs) and 6-31+G\* [55–58] basis sets. We included the six nearest cations to each Pd(dmit)<sub>2</sub> tetramer; benchmarking revealed that the calculated exchange interactions are

TABLE I. Our BS-DFT Heisenberg exchange interactions of  $\text{Et}_n\text{Me}_{4-n}\text{X}[\text{Pd}(\text{dmit})_2]_2$  (the compounds are listed here according to their values of  $X$  and  $n$ ).  $J_B$  is much larger than  $J_r$  and  $J_S$  in all materials. The interlayer exchange coupling  $J_z$  is very small. See Fig. 1 for the directions of the other couplings in the lattice.

Compound ( $X$ - $n$ )	$J_B$ (K)	$J_r$ (K)	$J_S$ (K)	$J_z$ (K)
Sb-0	320	145	86	-0.01
Sb-1	382	129	111	0.06
As-0	370	110	116	-0.02
As-1	353	129	100	<0.01
As-2	374	130	98	-0.01
N-0	352	131	143	0.04
P-1	499	195	148	5

well converged at this cluster size. Further details of our DFT calculations, including functional comparisons with different amounts of Hartree-Fock exchange and all  $\langle S^2 \rangle$  values, are included in the Supplemental Material [47]. We used a collection of experimental crystal structures [59].

Our BS-DFT calculations reveal three significant, pairwise, antiferromagnetic, nearest-neighbor couplings, shown in Table I and Fig. 1. The largest exchange coupling  $J_B$  (along the stacking direction in Fig. 1) is significantly larger than the others in all cases. Hence, our Heisenberg model is quasi-one-dimensional. For the two smaller (interchain) couplings, we make a change of variables to the average of the interchain couplings,  $\bar{J}_y = \frac{1}{2}(J_S + J_r)$ , and their difference,  $\delta J_y = J_r - J_S$ . Figure 2 shows a plot of  $\bar{J}_y$  and  $|\delta J_y| + |J_z|$  for each compound.

The interlayer couplings ( $J_z$ —perpendicular to the axes in Fig. 1) are all less than  $0.01J_B$ . However, they are unfrustrated and therefore have a non-negligible contribution to the

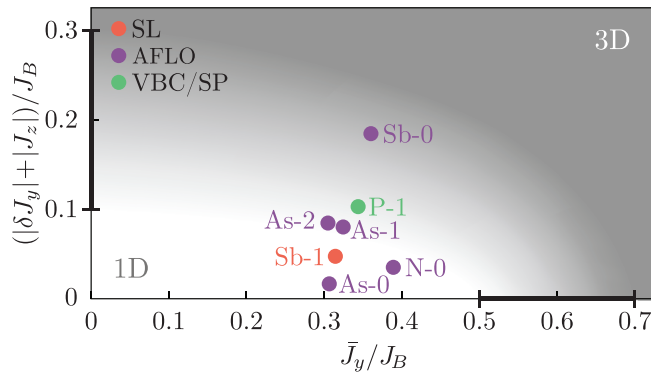


FIG. 2. BS-DFT results for the frustrated interstack interaction,  $\bar{J}_y = \frac{1}{2}(J_S + J_r)$ , and the unfrustrated  $|\delta J_y| + |J_z| = |J_r - J_S| + |J_z|$ , in units of the coupling along the stack direction,  $J_B$  (see Fig. 1). The marks on the axes indicate cutoffs for the validity of the CRPA for each interaction. The upper bounds indicate the most optimistic value in the literature, whereas the lower bounds indicate the most pessimistic value [60–67]. The shading is a guide to the eye based on these bounds. The colors differ based on the ground state of the compound according to the experimental literature: antiferromagnetic long-range order (AFLO), valence-bond crystal (VBC) or spin-Peierls (SP), and spin liquid (SL).

magnetic behavior. P-1 has the largest  $J_z$  by far, i.e., 5 K, which is interesting since it is the only compound purported to have a valence-bond crystal (VBC) or spin-Peierls (SP) ground state [1,6,7]. The quasi-1D picture naturally gives rise to a spin-Peierls ground state [68], whereas a 2D picture would suggest a VBC. Experimentally, these are difficult to distinguish. The important difference is that in a SP distortion, spin-phonon coupling and lattice distortion are essential ingredients of the mechanism, whereas the VBC is a fundamentally electronic effect and any lattice distortion is parasitic and driven by the spin-phonon coupling only on the lowering of the symmetry of the electrons. It is therefore interesting to note that the VBC/SP ground state is only observed in P-1—the only  $x$ -[Pd(dmit)<sub>2</sub>]<sub>2</sub> material that does *not* form the bilayer solid crossing structure. A lattice distortion would be strongly energetically disfavored in the solid crossing structure as there is an inherent elastic frustration between distortions along the (1,1,0) and (1, $\bar{1}$ ,0) directions in alternate layers [1]. Hence, this elastic distortion may suppress the VBC/SP phase. This suggests that there is an SP distortion rather than a VBC state in P-1 and thus that the  $x$ -[Pd(dmit)<sub>2</sub>]<sub>2</sub> materials are quasi-1D.

In a triangular, quasi-1D lattice, there are two interesting limits to consider: when the lattice becomes perfectly frustrated,  $\delta J_y$  and  $J_z \rightarrow 0$ , and when there is no geometrical frustration,  $J_S \rightarrow 0$  or  $J_r \rightarrow 0$ . In the first case, the model becomes perfectly isosceles with two equal interchain couplings,  $J_S = J_r = \bar{J}_y$ . Quantum Monte Carlo, exact diagonalization, density matrix renormalization group (DMRG), and other numerical calculations have shown that this model exhibits quasi-one-dimensional behavior for  $\bar{J}_y/J_B < 0.7$  [60–66]. In the second case, we have a cuboidal lattice with interchain couplings  $|\delta J_y|$  and  $J_z$ . This model, studied extensively by Schulz [39], exhibits quasi-one-dimensional behavior for  $(|\delta J_y| + |J_z|)/J_B < 0.3$  according to RPA calculations [67]. These limits are indicated on the axes of Fig. 2, where we find that the quasi-1D nature of the exchange couplings is evident in all compounds. Our calculations reveal that  $\bar{J}_y$  is always below  $0.4J_x$  and the sum of the unfrustrated interactions,  $|\delta J_y| + |J_z|$ , is below  $0.1J_x$ —only Sb-0 is anywhere near these limits, as it is less strongly frustrated than the other materials. We conclude that all compounds can be described by quasi-one-dimensional models.

### Comparison to previous first-principles studies

The couplings calculated in other first-principles studies of  $x$ -[Pd(dmit)<sub>2</sub>]<sub>2</sub> also reflect a quasi-1D character. As discussed above, most previous studies report monomer and dimer tight-binding parameters based on band structure methods (including the use of Wannier functions). In the large  $U$  limit,  $J_{ij}^{\text{SE}} \approx 4t_{ij}^2/U$ , where  $t_{ij}$  is the tight-binding transfer integral and  $U$  is the effective on-site Coulomb repulsion. This leads to  $\bar{J}_y^{\text{SE}}/J_B^{\text{SE}} \approx (t_S^2 + t_r^2)/(2t_B^2)$  and  $\delta J_y^{\text{SE}}/J_B^{\text{SE}} \approx (t_S^2 - t_r^2)/t_B^2$ . In Table II, we list these values from three previous studies; Misawa *et al.* [21], Tsumuraya *et al.* [19], and Scriven and Powell [18]. Most fit within the 1D region in Fig. 2 ( $\bar{J}_y^{\text{SE}}/J_B^{\text{SE}} \lesssim 0.7$ ;  $\delta J_y^{\text{SE}}/J_B^{\text{SE}} \lesssim 0.3$ ). Tsumuraya *et al.* [19] also find weak hopping between the layers, in agreement with our findings.

TABLE II. Previous results for interdimer superexchange based on DFT band structure calculations. Most of these models lie in or close to a weakly coupled chain regime ( $\bar{J}_y^{\text{SE}}/J_B^{\text{SE}} \lesssim 0.7$ ;  $J_y^{\text{SE}}/J_B^{\text{SE}} \lesssim 0.3$ ).

Ref.	$\bar{J}_y^{\text{SE}}/J_B^{\text{SE}}$	$\delta J_y^{\text{SE}}/J_B^{\text{SE}}$
[17]	0.62	0.14
[18]	0.65–0.90	0.13–0.28
[19]	0.45–0.62	0.02–0.35
[20]	0.49–0.80	0.19–0.30
[21]	0.44–0.55	0.01–0.16

We find that

$$\begin{aligned} \bar{J}_\perp(\mathbf{k}) &= J_r \cos\left(k_y - \frac{k_x}{2}\right) + J_s \cos\left(k_y + \frac{k_x}{2}\right) + J_z \cos(k_z) \\ &= 2\bar{J}_y \cos(k_y) \cos\left(\frac{k_x}{2}\right) + \delta J_y \sin(k_y) \sin\left(\frac{k_x}{2}\right) + J_z \cos(k_z), \end{aligned} \quad (4)$$

where, in the second line, we have used our change of variables defined above.

The dynamical susceptibility for a single Heisenberg chain around  $k_x = k_0 + \pi \approx \pi$  has been calculated from a combination of the Bethe ansatz and field theory techniques [71–75],

$$\chi_{1D}(\omega, k_0, T) = -\frac{\sqrt{\ln(\Lambda/T)} \Gamma\left(\frac{1}{4} - i\frac{\omega - uk_0}{4\pi T}\right) \Gamma\left(\frac{1}{4} - i\frac{\omega + uk_0}{4\pi T}\right)}{2t(2\pi)^{3/2} \Gamma\left(\frac{3}{4} - i\frac{\omega - uk_0}{4\pi T}\right) \Gamma\left(\frac{3}{4} - i\frac{\omega + uk_0}{4\pi T}\right)}, \quad (5)$$

where  $k_0 = k_x - \pi$ ,  $\Gamma(x)$  is the Euler gamma function,  $u = \frac{\pi}{2}J_x b_0$  is the spin velocity,  $b_0$  is the interdimer separation along the  $x$  direction in Fig. 1, and  $\Lambda/J_B \simeq 24.27$  [76].

We determine the Néel ordering temperature  $T_N$  by considering the condition for a zero frequency pole in Eq. (3). This occurs when

$$2\bar{J}_\perp(\mathbf{k})\chi_{1D}(0, k_x, t)|_{T=T_N} = 1. \quad (6)$$

This instability will occur at the maximum of  $\bar{J}_\perp(\mathbf{k})\chi_{1D}(0, k_x, T)$ . The presence of interchain couplings will shift this maximum to an incommensurate wave number, with the resulting order occurring at  $k_x = \pi + k_0$ . In this case, we find the maximum occurs when  $k_y = \arctan 2\{-\delta J_y \cos(k_0/2), [2\bar{J}_y \sin(k_0/2)]\}$ , where  $\arctan 2(y, x)$  is the two-argument arctangent, which returns the angle for the point  $(x, y)$  defined positively from the  $x$  axis. A numerical solution of this condition using our BS-DFT results for  $\bar{J}_y$ ,  $\delta J_y$ , and  $J_z$  gives the Néel temperatures shown in Table III.

For all compounds in Table III, we found  $k_0 < 10^{-12}$ . Taking the limit  $k_0 \rightarrow 0$  in Eq. (6) returns

$$T_N = 0.5558(|J_z| + |\delta J_y|) \sqrt{\ln\left(\frac{\Lambda}{T_N}\right)}. \quad (7)$$

This takes the same form as the prediction for coupled chains with unfrustrated, bipartite interchain couplings of magnitude  $\delta J_y$  along the  $y$  axis and  $J_z$  along the  $z$  axis [39]—demonstrating that  $\delta J_y$  simply acts as an unfrustrated coupling, while the frustrated contribution  $\bar{J}_y$  has no effect [since Eq. (7) is independent of  $\bar{J}_y$ ].

### III. CALCULATION OF NÉEL TEMPERATURE WITH THE CRPA

The CRPA expression for the three-dimensional dynamical magnetic susceptibility of a lattice of weakly coupled chains is [39,40,69,70]

$$\chi_{\text{CRPA}}(\omega, \mathbf{k}, T) = \frac{\chi_{1D}(\omega, k_x, T)}{1 - 2\bar{J}_\perp(\mathbf{k})\chi_{1D}(\omega, k_x, T)}, \quad (3)$$

where  $\chi_{1D}(\omega, k_x, T)$  is the dynamical susceptibility for a single Heisenberg chain,  $\bar{J}_\perp(\mathbf{k})$  is the Fourier transform of the interchain coupling, and  $\mathbf{k} = (k_x, k_y, k_z)$  is the crystal momentum along the axes in Fig. 1 in units of the inverse lattice spacing.

Figure 3 shows a plot of the Néel temperature from Eq. (7) with the numerical results for each material indicated as points. The numerical results match those from Eq. (7) perfectly. Comparing our results with experiment in Table III, our estimates of  $T_N$  are the same order of magnitude as the experimentally measured values. In general, our  $T_N$  values are higher than the experimental value. For example, if our model was qualitatively correct, the spin-liquid candidate

TABLE III. Calculated Néel temperatures of  $\text{Et}_n\text{Me}_{4-n}\text{X}[\text{Pd}(\text{dmit})_2]_2$  compounds that are experimentally confirmed to have a ground state with antiferromagnetic long-range order (AFLO), along with the spin-liquid (SL) candidate, Sb-1. These values are based on nearest-neighbor coupling parameters in Table I and compared with experimental measurements. We find Néel temperatures of the correct order of magnitude. Disagreements between our theory and experiment could point to the importance of higher-order spin processes, such a ring exchange [38,77–79].

Compound ( $X$ - $n$ )	Calc. $T_N$ (K)	Expt. $T_N$ (K)
As-0	8.7	35 [3]
As-1	37	23 [4]
As-2	41	18 [3]
N-0	17	12 [5]
Sb-0	70	18 [3]
Sb-1	24	<0.02 (SL) [10]



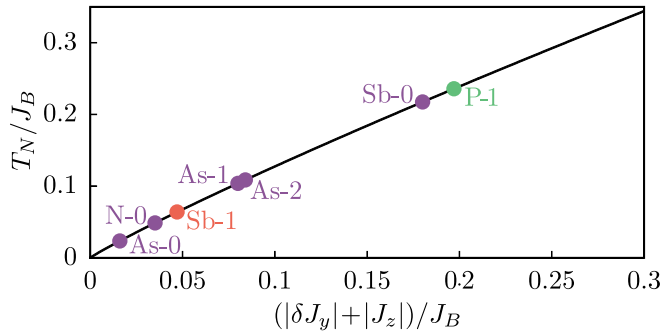


FIG. 3. Relationship between  $T_N$  and the sum of the unfrustrated couplings,  $|\delta J_y| + |J_z|$ . Numerical calculations from Table III are shown as labeled points with the same coloring as in Fig. 2. The black line is Eq. (7), which passes perfectly through the numerical results. This demonstrates that taking the limit  $k_0 \rightarrow 0$  does not affect the results and, hence, Eq. (7) is an accurate representation of the full numerical solution to Eq. (6) in this regime.

Sb-1 would have  $T_N \approx 0$ . However, we find even lower Néel temperatures for As-0 and N-0. Our overestimation of  $T_N$  could point to the importance of higher-order spin processes, such as a ring exchange [38,77–79], that have different magnitudes in different materials—consistent with the different pressures/strains required to drive different materials into metallic/superconducting states. Nevertheless, a theory based on first-principles calculations that gives quantitatively reasonable predictions for organic charge transfer salts is a significant advance.

#### IV. DISCUSSION OF EXPERIMENTAL RESULTS

We recently proposed that the “spin-liquid” state observed in Sb-1 could be a remnant of a Tomonaga-Luttinger liquid phase [38]. This prediction is consistent with the observed linear heat capacity. This picture also provides a natural explanation of the broad features observed around 1–4 K in <sup>13</sup>C nuclear magnetic resonance (NMR) relaxation rates and heat capacity in terms of short-range interchain correlations. Finally, as detailed in [38], it provides a simple solution to the recent controversy surrounding thermal conductivity measurements of Sb-1 [80–85] because the magnetic and phononic intrachain heat conductivities behave very differently.

Tamura and Kato [36] fit magnetic susceptibility measurements with a triangular model ( $J_B = J_r = J_S$ ) and Nakamura *et al.* [86] interpret their Raman scattering measurements in the  $J_B \approx J_S > J_r$  regime. However, neither measurement strongly excludes a quasi-one-dimensional picture. On the other hand, an electron paramagnetic resonance (EPR) study

by Nakamura *et al.* [3] found a close relationship between the Néel temperatures and the interstack interactions ( $J_S$  and  $J_r$ )—consistent with our finding that the magnetic exchange interactions are quasi-1D and that  $T_N$  is dominated by interchain interactions, as in Eq. (7) and Fig. 3.

Thus, a quasi-1D picture is consistent with the existing experimental literature and provides a natural explanation of why only P-1 has a SP distortion, see Sec. II. However, more detailed experimental tests of our proposal are needed and we hope that this manuscript will motivate studies to test the difference between quasi-1D and quasi-2D behavior in these materials. Given that these compounds are soft, it may be illuminating to conduct magnetic measurements on samples under pressure or uniaxial strain.

#### V. CONCLUSIONS

We have used BS-DFT, an atomistic approach, to parametrize a Heisenberg model for several materials in the  $\text{Et}_n\text{Me}_{4-n}\text{X}[\text{Pd}(\text{dmit})_2]_2$  family. This revealed a frustrated scalene triangular lattice where the largest coupling along the stacking direction is nearly three times larger than the others. We showed that in the relevant quasi-one-dimensional limit, the difference in the interchain coupling acts identically to an unfrustrated interchain coupling and favors long-range magnetic order. This is the role of geometric frustration in a quasi-1D triangular lattice; the effective interchain coupling, which is the main driver for magnetic order, is reduced significantly due to competing interactions. We calculate the Néel temperatures in this picture and find that they are the same order of magnitude as experimental values, but are overestimates in most cases. This could indicate the importance of higher-order spin processes, such as a ring exchange, in the  $x$ -[Pd(dmit)<sub>2</sub>]<sub>2</sub> family.

Treating these compounds as quasi-1D is consistent with the existing experimental literature and provides a natural explanation of why only P-1 has a SP distortion. In this picture, geometrical frustration and strong electron correlations still play a large role. In particular, frustration increases the effective one-dimensionality ( $\delta J_y \ll J_r, J_S$ ).

More broadly, the demonstration that we can get correct orders of magnitude for the Néel temperatures in the  $x$ -[Pd(dmit)<sub>2</sub>]<sub>2</sub> materials brings us close to achieving the long-held goal of making quantitative predictions for electronic phenomena in strongly correlated electron materials.

#### ACKNOWLEDGMENTS

We thank Amie Khosla and Ross McKenzie for helpful conversations. This work was supported by the Australian Research Council through Grants No. DP160100060 and No. DP181006201.

- [1] B. J. Powell and R. H. McKenzie, *Rep. Prog. Phys.* **74**, 056501 (2011).  
 [2] K. Kanoda and R. Kato, *Annu. Rev. Condens. Matter Phys.* **2**, 167 (2011).

- [3] T. Nakamura, T. Takahashi, S. Aonuma, and R. Kato, *J. Mater. Chem.* **11**, 2159 (2001).  
 [4] R. Kato, A. Tajima, A. Nakao, and M. Tamura, *J. Am. Chem. Soc.* **128**, 10016 (2006).

- [5] A. Kobayashi, A. Miyamoto, R. Kato, A. Sato, and H. Kobayashi, *Bull. Chem. Soc. Jpn.* **71**, 997 (1998).
- [6] M. Tamura, A. Nakao, and R. Kato, *J. Phys. Soc. Jpn.* **75**, 093701 (2006).
- [7] Y. Shimizu, H. Akimoto, H. Tsujii, A. Tajima, and R. Kato, *Phys. Rev. Lett.* **99**, 256403 (2007).
- [8] A. Nakao and R. Kato, *J. Phys. Soc. Jpn.* **74**, 2754 (2005).
- [9] M. Tamura, K. Takenaka, H. Takagi, S. Sugai, A. Tajima, and R. Kato, *Chem. Phys. Lett.* **411**, 133 (2005).
- [10] T. Itou, S. Oyamada, A. Maegawa, and R. Kato, *Nat. Phys.* **6**, 673 (2010).
- [11] T. Itou, K. Yamashita, M. Nishiyama, A. Oyamada, S. Maegawa, K. Kubo, and R. Kato, *Phys. Rev. B* **84**, 094405 (2011).
- [12] R. Kato and C. Hengbo, *Crystals* **2**, 861 (2012).
- [13] Y. Zhou, K. Kanoda, and T.-K. Ng, *Rev. Mod. Phys.* **89**, 025003 (2017).
- [14] R. Kato, *Chem. Rev.* **104**, 5319 (2004).
- [15] R. Yamamoto, Y. Yanagita, T. Namaizawa, S. Komuro, T. Furukawa, T. Itou, and R. Kato, *Phys. Rev. B* **97**, 224502 (2018).
- [16] T. Itou, A. Oyamada, S. Maegawa, M. Tamura, and R. Kato, *Phys. Rev. B* **77**, 104413 (2008).
- [17] K. Nakamura, Y. Yoshimoto, and M. Imada, *Phys. Rev. B* **86**, 205117 (2012).
- [18] E. P. Scriven and B. J. Powell, *Phys. Rev. Lett.* **109**, 097206 (2012).
- [19] T. Tsumuraya, H. Seo, M. Tsuchiizu, R. Kato, and T. Miyazaki, *J. Phys. Soc. Jpn.* **82**, 033709 (2013).
- [20] A. C. Jacko, L. F. Tocchio, H. O. Jeschke, and R. Valentí, *Phys. Rev. B* **88**, 155139 (2013).
- [21] T. Misawa, K. Yoshimi, and T. Tsumuraya, *Phys. Rev. Research* **2**, 032072(R) (2020).
- [22] W. Kohn and L. J. Sham, *Phys. Rev.* **140**, A1133 (1965).
- [23] R. O. Jones and O. Gunnarsson, *Rev. Mod. Phys.* **61**, 689 (1989).
- [24] J. P. Perdew, *Intl. J. Quantum Chem.* **28**, 497 (1985).
- [25] R. Adler, C.-J. Kang, C.-H. Yee, and G. Kotliar, *Rep. Prog. Phys.* **82**, 012504 (2018).
- [26] J. P. Malrieu, R. Caballol, C. J. Calzado, C. de Graaf, and N. Guihéry, *Chem. Rev.* **114**, 429 (2014).
- [27] I. P. R. Moreira, F. Illas, and R. L. Martin, *Phys. Rev. B* **65**, 155102 (2002).
- [28] S. Zein, M. Poor Kalthor, L. F. Chibotaru, and H. Chermette, *J. Chem. Phys.* **131**, 224316 (2009).
- [29] J. J. Phillips and J. E. Peralta, *J. Chem. Theory Comput.* **8**, 3147 (2012).
- [30] E. Coulaud, N. Guihéry, J.-P. Malrieu, D. Hagebaum-Reignier, D. Siri, and N. Ferré, *J. Chem. Phys.* **137**, 114106 (2012).
- [31] M. H. Whangbo, H.-J. Koo, and D. Dai, *J. Solid State Chem.* **176**, 417 (2003).
- [32] I. d. P. R. Moreira and F. Illas, *Phys. Chem. Chem. Phys.* **8**, 1645 (2006).
- [33] M.-H. Whangbo, H.-J. Koo, and R. K. Kremer, *Molecules* **26**, 531 (2021).
- [34] X. Li, H. Yu, F. Lou, J. Feng, M.-H. Whangbo, and H. Xiang, *Molecules* **26**, 803 (2021).
- [35] P. Hohenberg and W. Kohn, *Phys. Rev.* **136**, B864 (1964).
- [36] M. Tamura and R. Kato, *J. Phys.: Condens. Matter* **14**, L729 (2002).
- [37] W. Zheng, R. R. P. Singh, R. H. McKenzie, and R. Coldea, *Phys. Rev. B* **71**, 134422 (2005).
- [38] E. P. Kenny, G. David, N. Ferré, A. C. Jacko, and B. J. Powell, *Phys. Rev. Mater.* **4**, 044403 (2020).
- [39] H. J. Schulz, *Phys. Rev. Lett.* **77**, 2790 (1996).
- [40] M. Bocquet, F. H. L. Essler, A. M. Tsvelik, and A. O. Gogolin, *Phys. Rev. B* **64**, 094425 (2001).
- [41] E. P. Kenny, A. C. Jacko, and B. J. Powell, *Angew. Chem. Intl. Ed.* **58**, 15082 (2019).
- [42] P. W. Anderson, *Phys. Rev.* **79**, 350 (1950).
- [43] L. Noodleman, *J. Chem. Phys.* **74**, 5737 (1981).
- [44] J.-M. Mouesca, in *Metallo-proteins: Methods and Protocols*, edited by J. C. Fontecilla-Camps and Y. Nicolet (Humana Press, Totowa, NJ, 2014), Chap. 15, pp. 269–296.
- [45] K. Yamaguchi, F. Jensen, A. Dorigo, and K. Houk, *Chem. Phys. Lett.* **149**, 537 (1988).
- [46] N. Ferré, N. Guihéry, and J.-P. Malrieu, *Phys. Chem. Chem. Phys.* **17**, 14375 (2015).
- [47] See Supplemental Material at <http://link.aps.org/supplemental/10.1103/PhysRevMaterials.5.084412> for details regarding our DFT calculations and benchmarking.
- [48] M. J. Frisch *et al.*, *computer code Gaussian 09 Revision E.01* (Gaussian Inc. Wallingford, CT, 2009).
- [49] A. D. Becke, *J. Chem. Phys.* **98**, 5648 (1993).
- [50] P. J. Stephens, F. J. Devlin, C. F. Chabalowski, and M. J. Frisch, *J. Phys. Chem.* **98**, 11623 (1994).
- [51] T. H. Dunning Jr. and P. J. Hay, in *Methods of Electronic Structure Theory*, Vol. 2, 3rd. ed., edited by H. F. Schaefer (Springer, Boston, 1977), Chap. 1, pp. 1–27.
- [52] P. J. Hay and W. R. Wadt, *J. Chem. Phys.* **82**, 270 (1985).
- [53] W. R. Wadt and P. J. Hay, *J. Chem. Phys.* **82**, 284 (1985).
- [54] P. J. Hay and W. R. Wadt, *J. Chem. Phys.* **82**, 299 (1985).
- [55] R. Ditchfield, W. J. Hehre, and J. A. Pople, *J. Chem. Phys.* **54**, 724 (1971).
- [56] W. J. Hehre, R. Ditchfield, and J. A. Pople, *J. Chem. Phys.* **56**, 2257 (1972).
- [57] P. C. Hariharan and J. A. Pople, *Theoret. Chim. Acta* **28**, 213 (1973).
- [58] M. M. Francl, W. J. Pietro, W. J. Hehre, J. S. Binkley, M. S. Gordon, D. J. DeFrees, and J. A. Pople, *J. Chem. Phys.* **77**, 3654 (1982).
- [59] R. Kato (private communication, 2013).
- [60] M. Q. Weng, D. N. Sheng, Z. Y. Weng, and R. J. Bursill, *Phys. Rev. B* **74**, 012407 (2006).
- [61] S. Yunoki and S. Sorella, *Phys. Rev. B* **74**, 014408 (2006).
- [62] Y. Hayashi and M. Ogata, *J. Phys. Soc. Japan* **76**, 053705 (2007).
- [63] T. Pardini and R. R. P. Singh, *Phys. Rev. B* **77**, 214433 (2008).
- [64] H. C. Jiang, M. Q. Weng, Z. Y. Weng, D. N. Sheng, and L. Balents, *Phys. Rev. B* **79**, 020409(R) (2009).
- [65] D. Heidarian, S. Sorella, and F. Becca, *Phys. Rev. B* **80**, 012404 (2009).
- [66] T. Tay and O. I. Motrunich, *Phys. Rev. B* **81**, 165116 (2010).
- [67] C. Yasuda, S. Todo, K. Hukushima, F. Alet, M. Keller, M. Troyer, and H. Takayama, *Phys. Rev. Lett.* **94**, 217201 (2005).
- [68] M. C. Cross and D. S. Fisher, *Phys. Rev. B* **19**, 402 (1979).
- [69] D. J. Scalapino, Y. Imry, and P. Pincus, *Phys. Rev. B* **11**, 2042 (1975).

- [70] F. H. L. Essler, A. M. Tsvelik, and G. Delfino, *Phys. Rev. B* **56**, 11001 (1997).
- [71] H. Z. Bethe, *Z. Phys.* **71**, 205 (1931).
- [72] H. J. Schulz and C. Bourbonnais, *Phys. Rev. B* **27**, 5856(R) (1983).
- [73] H. J. Schulz, *Phys. Rev. B* **34**, 6372 (1986).
- [74] V. Barzykin, *J. Phys.: Condens. Matter* **12**, 2053 (2000).
- [75] A. M. Tsvelik, *Quantum Field Theory in Condensed Matter Physics*, Vol. 2 (Cambridge University Press, Cambridge, UK, 2003).
- [76] V. Barzykin, *Phys. Rev. B* **63**, 140412(R) (2001).
- [77] M. Holt, B. J. Powell, and J. Merino, *Phys. Rev. B* **89**, 174415 (2014).
- [78] J. Merino, M. Holt, and B. J. Powell, *Phys. Rev. B* **89**, 245112 (2014).
- [79] O. I. Motrunich, *Phys. Rev. B* **72**, 045105 (2005).
- [80] M. Yamashita, N. Nakata, Y. Senshu, M. Nagata, H. M. Yamamoto, R. Kato, T. Shibauchi, and Y. Matsuda, *Science* **328**, 1246 (2010).
- [81] M. Yamashita, Y. Sato, T. Tominaga, Y. Kasahara, S. Kasahara, H. Cui, R. Kato, T. Shibauchi, and Y. Matsuda, *Phys. Rev. B* **101**, 140407(R) (2020).
- [82] P. Bourgeois-Hope, F. Laliberté, E. Lefrançois, G. Grissonnanche, S. R. de Cotret, R. Gordon, S. Kitou, H. Sawa, H. Cui, R. Kato, L. Taillefer, and N. Doiron-Leyraud, *Phys. Rev. X* **9**, 041051 (2019).
- [83] J. M. Ni, B. L. Pan, B. Q. Song, Y. Y. Huang, J. Y. Zeng, Y. J. Yu, E. J. Cheng, L. S. Wang, D. Z. Dai, R. Kato, and S. Y. Li, *Phys. Rev. Lett.* **123**, 247204 (2019).
- [84] M. Yamashita, *J. Phys. Soc. Jpn.* **89**, 086002 (2020).
- [85] H. Fukuyama, *J. Phys. Soc. Jpn.* **89**, 086001 (2020).
- [86] Y. Nakamura, R. Kato, and H. Kishida, *J. Phys. Soc. Jpn.* **84**, 044715 (2015).